



Numerical Investigations on Alternate Droplet Formation in Microfluidic Devices

Sripada Raja¹ · M. N. Satyanarayan¹ · G. Umesh¹ · Gopalkrishna Hegde²

Received: 13 March 2021 / Accepted: 15 November 2021 / Published online: 13 December 2021
© The Author(s), under exclusive licence to Springer Nature B.V. 2021

Abstract

We present numerical investigations on generating droplets in both single and double T-junction microfluidic devices using the Volume of Fluid (VOF) method. We validate our 2D simulation results with an experimental data reported in the past. The average pressure in the channel increases by 6% and capillary number by 16% for an increase in the width of side-channel from 50 μm to 100 μm in a single T-junction device. Similar increase in average pressure and capillary number is seen, for the increase in the width of one of the side channel in double T-junction device. The temporal variation of pressure in both the side channels shows that the pressure is lesser in the wider side channel. The average pressure in the channel decreases by 75% and capillary number by 15% for an increase in width of the main channel from 50 μm to 100 μm in a single T-junction device. Similar decrease in average pressure and capillary number is seen for the increase in the width of the main channel in double T-junction device. A gradual increase in the width of the main channel shows that, droplets generated in alternate regime when the width of the main channel is 1.4 times the width of side channel. In this regime, the temporal variation in pressure show a periodic change in both the side channel. Finally, in double T-junction device, the addition of surfactant has no significant effect on droplet generation in merging regime but it is seen in alternate regime.

Keywords Droplet Microfluidics · Double T-junction device · Alternate droplet generation · Volume of Fluid method

Introduction

Droplet Microfluidics has advanced in the last two decades to a stage wherein programmed generation of monodispersed droplets, of nano-litre to pico-litre volumes, at the desired rate has become possible. The interest in this field is driven by a variety of novel applications such as protein crystallization (Zheng et al. 2004b), measurement of blood clotting time using anticoagulant drugs (Song et al. 2006), drug discovery (Brouzes et al. 2009), single-cell analysis (Kemna et al. 2012), encapsulation of microfibers in microdroplets for food processing, cosmetics, and pharmaceutical products (Nunes et al. 2013), synthesis of microcapsules (Kong et al. 2013; Datta et al. 2014; Lee et al. 2016), polymer chain reactions methods for DNA amplification (Zhang and Jiang

2016), encapsulating multicell organism (Beneyton et al. 2016). Droplet generation has been achieved using Microfluidic devices of mainly three types, viz. T-junctions (Li et al. 2012), Cross Junction (Seo et al. 2007), and Co-flow (Hong and Wang 2007; Li et al. 2020). In all these devices, droplet generation involves the flow of two immiscible liquids. The primary liquid is called the continuous phase liquid whose viscosity is μ_c and it flows with flowrate Q_c . The second liquid is called the dispersed phase liquid whose viscosity is μ_d . It flows with a flowrate Q_d . Interactions of the two immiscible liquids in the flow channel led to droplet formation by either Squeezing, Dripping, or Jetting mechanism. Sometimes droplets can also be generated in transition state such as Squeezing to dripping transition regime (Arias and Montlaur 2020). The mechanism that will dominate in any experiment will depend on parameters such as flow rates of the two liquids (Garstecki et al. 2006; Yan et al. 2012), the viscosity ratio ($\lambda = \mu_d/\mu_c$) (Nekouei and Vanapalli 2017), the aspect ratio of the channels (Yan et al. 2012; Gupta et al. 2014), and interfacial tension between the two fluids (Peng et al. 2011). For practical applications, it is important to generate droplets of the same volume. In the present investigation,

✉ Sripada Raja
sripadaraja@gmail.com

¹ Department of Physics, National Institute of Technology, Surathkal, Mangalore, Karnataka 575025, India

² BioSystems Sciences and Engineering, Indian Institute of Science, Bangalore 560012, India

we have investigated droplet generation in single and double T-junction device.

The ratio of viscous shear force to the interfacial tension determines the capillary number (C_a) of the system. C_a is dependent on viscosity, flowrate of the two liquids and interfacial tension between them. In the single T-junction device (Fig. 1a), dispersed phase liquid is passed from the side channel whereas, in the double T-junction device (Fig. 1b), it is passed from the two side channels inlets (SC1 and SC2) and the oil is passed through the main channel inlet. In the double T-junction device, the dispersed phase liquid in both the side channel meets at the junction and merge. The merged portion is pinched off due to the viscous shear force of oil. This droplet generation mechanism, in double T-junction device is termed as a “merging regime”. This is seen for $Ca < 0.024$ (Ngo et al. 2015; Surya et al. 2015). For $Ca \geq 0.024$, the dispersed phase liquid in the two side channels do not merge. Instead, they are generated well separated at the junction. This is termed as alternate droplet formation (ADF) regime or alternate regime. The droplet generation in alternate regime is seen to happen as follows: when the dispersed phase liquid from one of the side channels enters the main channel, it blocks the continuous phase liquid as it grows at the junction. Due to this, there is an increase in pressure upstream. A small volume of dispersed phase liquid breaks off to form the droplet. The dispersed phase liquid recoils back into the side channel and in the process, the dispersed phase liquid from another side-channel enters the main channel to form the droplet and this cycle continues (Yesiloz et al. 2015).

Several applications have been reported in the past using double T-junction devices. Droplets can be merged at the junction or away from it. It was demonstrated that with the addition of surfactant such as Span 80 at 0.5% (wt / wt) in mineral oil, the merging efficiency of water droplets were good (Um et al. 2008). During this process, the Q (Q_d/Q_c) was maintained between 0.1 to 0.6. Merging of droplets away from the junction is seen in double T-junction and Y-junction devices (side-channel is at 45° to the main channel) (Jin and Yoo 2012). In a similar device, water droplets were generated in mineral oil with different concentrations (0% to 5%) of Span 80 (Liu and Qin 2013). In this investigation, the merging efficiency was reduced with an increase in surfactant concentration up to 3% to 5% of surfactant concentration. It was demonstrated that droplets can also be merged with two T-junctions (two side channels are parallel to each other on the same side) for synthesizing inorganic–organic block copolymer (Hoang and Dien 2014). Using simulation, it was shown that the droplet generation in the merging regime in a double T-junction device can be understood by plotting pressure versus time (Han and Chen 2019a). In this study, pressure change with time shows that blocking time and breaking time of dispersed phase liquid increases with interfacial tension. Further, it was shown that the average pressure increases with the viscosity of continuous phase liquid and the frequency of droplet generation and average pressure increases with an increase in the flowrate of continuous phase liquid. They continued and presented the study on droplet merging by varying the angle between the side channel and the main channel between 30° to 150° (Han and Chen 2019b). The study showed that, smaller diameter of droplets were found when the

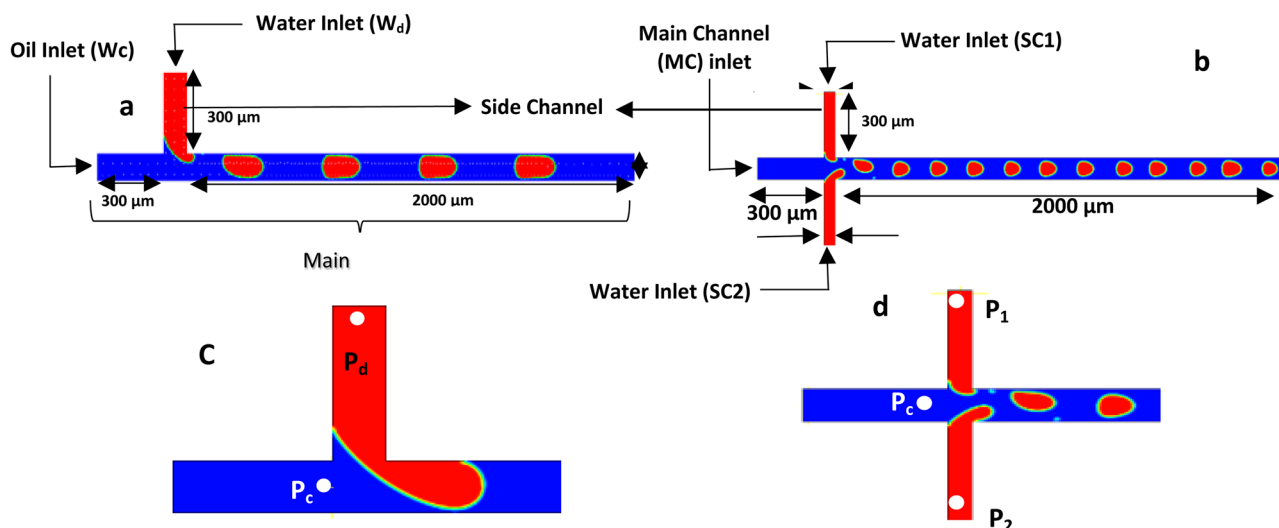


Fig. 1 Schematic of the droplet generating microfluidic devices. **a** Droplet formation in a single T-junction device, **b** Droplet formation in double T-junction device, **c** Representation of pressure determining

point P_c and P_d in single T-junction device, **d** Representation of pressure determining point P_c , P_1 , and P_2 in a double T-junction device

angle between the side and main channel is at 60° and when the channel height to width ratio is high.

The first study on the double T-junction device model was realised to produce droplets in different regimes namely merging, alternating, alternate-jetting, and jetting (Zheng et al. 2004a, b). A modified geometry was proposed and demonstrated producing alternate droplet generation, in various regimes to synthesise CdS nanoparticles (Hung et al. 2006). In this device, droplets of different volumes were produced from each side channel by controlling the flow rate of the dispersed phase liquid independently in the two side channels. Picolitre aqueous droplets were generated in a double T-junction device in an alternate regime (Fidalgo et al. 2007). In this device, a portion of the microchannel wall was made hydrophilic. Pair of droplets generated were merged when they reach the hydrophilic region in the microchannel and finally get trapped. A device with two T-junctions in tandem was developed to synthesis poly (lactide-co-glycolide) commonly known as PLGA (Hung et al. 2010). In this device, silicone oil was used as a continuous phase liquid and a side channel carried water and another side-channel carried PLGA. In applications involving cell encapsulation, the encapsulated cell may slip to continuous phase liquid. To avoid this, droplets of water and air bubbles were generated in a double T-junction device to locate the cell which is encapsulated (O'Brien et al. 2012). Monodispersed water-in-oil-in-water emulsion droplets were generated in Decane. Various surfactants such as Span 80, Span 85, SY Glyster CRC-75 were used as a surfactant at 1% concentration (wt/wt) were added to continuous phase liquid (Hirama and Torii 2015). One device contained both, a double T-junction and a Y-junction. In this device, initially the droplets were generated in an alternate regime. During this process, fluorescence microbeads were mixed in water (DMEM/ Cell culture solution) and passed through one of the side channels. This generated droplet pair (one droplet from each side channel constitutes droplet pair). The inclination of the side-channel at 45° to the main channel can also produce droplets in an alternate regime (Jin and Yoo 2012). Surya et al. further showed that the droplets were generated in the merging regime for $Ca < 0.024$ and alternate regime for Ca ranging between 0.028 to 0.13. The droplet generation mechanism was understood through simulations and the results were found to match within less than 15% of the error margin. A numerical study using double T-junction device shows, for different ratios of widths of side-channel to the main channel (Λ) (in the range 0.5, to 1.5) (Ngo et al. 2015). It was found that in merging regime, the pressure at point P_1 and P_2 are equal. The temporal variation of pressure in both side channel in alternate regime was demonstrated by an experiment with matching simulation results using a double T-junction device which has symmetric tapered side channels (Saqib et al. 2018).

Few investigations in the past on single T-junction device map the flow parameters like pressure and capillary number for varying width of the side and main channel. We adopt similar study to compare and emphasise related variations in double T-junction device. We investigate droplet generation mechanism in both symmetric and asymmetric double T-junction device. The addition of surfactant reduces the interfacial tension between the two fluids (Glawdel and Ren 2012; Tadros 2013) and alters the wetting conditions of dispersed phase liquid with the channel wall (Dreyfus et al. 2003; Bashir et al. 2014). Hence, we further investigate, droplet generation mechanism in merging and alternate regime in double T-junction device for increase in the surfactant concentration (Span 80) in mineral oil.

3D simulations may provide more accurate results, but they are computationally expensive. However, 2D simulations are no less, they also provide relevant information about droplet generation in microfluidic devices with good qualitative agreement with experimental data (Belousov et al. 2021). Recently, the advantages in adopting 2D simulations have been emphasized (Soroor et al. 2021). In any case, if 3D simulation were performed, the lateral wall effects would slightly be weakened. But this wouldn't affect the result significantly and would not make the results unreliable. The droplet break-up mechanism in 2D simulations resemble with that of 3D simulation (Leshansky and Pismen 2009) and in relevance to this, many studies in the past (Liu and Zhang 2009; Amaya-Bower and Lee 2011) and recently (Wojnicki et al. 2018; Nasser et al. 2019) have validated their 2D simulations with an experiment. The results are in good agreement. Considering these facts, we adopt 2D simulations in our study.

This paper reports the simulation performed on both single and double T-junction devices. Using the parameters such as, frequency of droplets generated, their length, the pressure at both the side and main channel inlets, and capillary number are noted for varying channel width in both single and double T-junction devices, a comparative study between single and double T-junction devices is investigated and results are presented. Further, we understand the droplet generation mechanism in double T-junction in merging and alternate regime for an increase in the concentration of surfactant (Span 80) in mineral oil. The results are presented by plotting pressure difference plots with time between the two side-channel inlets with time in double T-junction devices in merging and alternate regimes.

Numerical Model and Simulation

The single T-junction and double T-junction devices are schematically shown in Fig. 1a and b, respectively. Mineral oil is the continuous phase liquid (density $\rho = 840 \text{ kg/m}^3$

and viscosity $\eta = 24.1$ mPa-s) which flows through the main channel inlet and water is the dispersed phase liquid (density $\rho = 998$ kg/m³ and viscosity $\eta = 1$ mPa-s), which flows through the side channel. The fluid properties mentioned are at room temperature. The width of the side channel of the single T-junction device is W_d (Fig. 1a). Similarly, the width of the side channels of a double T-junction device is SC1 and SC2 (Fig. 1b).

The basic equations used in the simulation are listed below. The continuity equation for an incompressible fluid is given by (Vivek Ranade 2019)

$$(\rho_{avg} \overline{U''}) = 0 \tag{1}$$

And for the of motion for the fluid is given by,

$$\frac{\partial(\rho_{avg} \overline{U''})}{\partial t} + \nabla \cdot (\rho_{avg} \overline{U''U''}) = -\nabla P + \nabla \cdot \overline{\tau} + \overline{F}_{SF} \tag{2}$$

where $\overline{U''}$, P , ρ_{avg} , $\overline{\tau}$ and \overline{F}_{SF} are velocity, pressure, density (averaged), stress tensor and surface tension force respectively for the fluid. For Newtonian liquids which are incompressible, the shear stress is relative and proportional to the rate of strain tensor $\dot{\gamma}$ which is represented as,

$$\overline{\tau} = \dot{\gamma} \eta_{avg} = \eta_{avg} (\nabla \overline{U''} + \nabla \overline{U''}) \tag{3}$$

where η_{avg} is the averaged viscosity. For the two-component fluid being considered, we define the density and viscosity of the volume (averaged) in-terms of the fractional volume of the two immiscible fluids such as oil (V_o) and water (V_w) as follows (Vivek Ranade 2019).

$$\rho_{avg} = V_o \rho_o + (1 - V_w) \rho_w \tag{4}$$

$$\eta_{avg} = V_o \eta_o + (1 - V_w) \eta_w \tag{5}$$

where ρ_w, ρ_o , are the density and η_w and η_o are the viscosity of water and oil, respectively. The fractional volume (V_f) of the individual fluid phase is computed by resolving the following equation.

$$\frac{\partial V_f}{\partial t} + \overline{U''} \cdot \nabla V_f = 0 \tag{6}$$

“f” is the subscript that describes any of the two fluids. In each mesh element, the fractional volume of the two phases is conserved implying $\sum V_f = 1$. If $V_f = 0$, the specific mesh element is said to be empty of the f^{th} phase and $V_f = 1$ indicating that the element (cell) is loaded with the f^{th} phase. Thus, the two-phase interface is demarcated by the value of the fractional volume.

We adopt the model of continuum surface force (CSF) and accordingly define the interfacial tension force (\overline{F}_{SF}) which is volumetric and is represented as

$$\overline{F}_{SF} = \sigma \left(\frac{\rho R_n \nabla V_0}{0.5(\rho_o + \rho_w)} \right) \tag{7}$$

where “ σ ” is the coefficient of interfacial tension among two liquids and R_n the radius of curvature of the droplet is expressed in terms as

$$R_n = -\nabla \cdot \hat{n} = \frac{1}{|\vec{n}|} \left[\left(\frac{\vec{n}}{|\vec{n}|} \cdot \nabla \right) |\vec{n}| - (\nabla \cdot \vec{n}) \right] \tag{8}$$

where \hat{n} is the component normal to the droplet surface. Considering the VOF formulation the surface normal $|\vec{n}|$ is expressed as the gradient of fractional volume phase at the interface which can be written as

$$\vec{n} = \nabla \cdot V_f \tag{9}$$

The force due to interfacial tension is implemented by piecewise linear interface calculation (Brackbill et al. 1992). The effects of wall adhesion are considered by providing the necessary value for the contact angle with the channel wall (Θ_w). Therefore, the surface normal at the reference cell next to the wall is given by,

$$\hat{n} = \hat{n}_w \cos \theta_w + \hat{m}_w \sin \theta_w \tag{10}$$

where \hat{n}_w and \hat{m}_w are the unit vectors which are normal and tangential to the wall, respectively.

The Sequence of Simulation Settings

Computational Model and VOF Simulation Settings

Simulations were performed using ANSYS Fluent software in which the Level Set method (LSM), and the Volume of fluid model (VOF) are used in combination. In practical applications, there are two ways to flow the liquid into in the device, i) using pressurised tanks in which the flowrate can be controlled and, ii) using syringe pumps. Both these methods can provide a constant flowrate for the two liquids in the microchannel. Many literatures in the past set velocity at its inlet. We continue to use velocity inlets in our computational model. The computational model for single and double T-junction devices is shown in Fig. 1a and b, respectively. In a single T-junction device, the continuous phase and dispersed phase liquids are passed through the main and side channels, respectively. In the case of a double

T-junction device, the dispersed and continuous phase liquids are passed through the two side and main channels, respectively. The velocity of the continuous phase (V_c) and dispersed phase (V_d) liquids are fixed to 0.02 m/s and 0.01 m/s, respectively in our study (except in Sect. 4.3.1 to study the droplet generation in merging regime). Both the devices have a normal outflow boundary condition set at the outlet.

To compute the coupling effect between the pressure and fluid velocity in the momentum equation, the “Pressure Implicit with Splitting of Operators (PISO)” scheme in ANSYS fluent simulation software is used. False currents arising due to the mismatch between pressure and interfacial tension forces were removed using the Pressure staggering option (PRESTO). The implicit method of the first order has been adopted for the discretization of time derivatives. The criterion for the convergence of continuity equation, the equations for X-momentum and Y-momentum, and the computation of the Level set function were set as attaining a minimum residual of 0.001. This implies that, during the computation of any residual falls below 0.001, then the solution is taken to have converged. The flowtime for the computation is set to be 0.1 s with a step size of 5 μ sec to maintain the global Courant number below 0.2. This ensures that the time step increment and its duration in the transport equations lead to accurate tracking of transportation of the fluid element across a control volume. The flow rate of the two liquids is specified at the respective inlets and the normal outflow condition is specified at the common outlet. Simulations are performed considering the inner surface of the channel wall to be completely wetted by the continuous phase liquid. Hence, the no-slip boundary condition is employed for the continuous phase liquid. The change in the interfacial tension and contact angle due to the addition of surfactant at various concentration is considered during the simulation from experimental measurements (Bashir et al. 2014). Hexahedral mesh elements are adopted. To determine the appropriate size of the mesh element, we computed the droplet length for mesh sizes of 4 μ m, 2 μ m, and 1 μ m. The droplet length changed by less than 1% for mesh size of 2 μ m as compared to that for 1 μ m. Hence, all the simulations were performed with a mesh element size of 2 μ m. The length kept for the microchannel was seen to be adequate for the droplet to be fully developed.

Analysis

Influence of Width of Side-Channel on Droplet Generation

The droplet generation in a single T-junction device is analysed by varying the width of the side channel from 50 μ m to 100 μ m (Fig. 1a) while the width of the main channel is fixed to 100 μ m. The average pressure at point P_c and P_d

(Fig. 1c), the droplet length, its generating frequency, and capillary number are reported. The study is repeated on a double T-junction device. The width of only one of the side channels (SC2) (Fig. 1b) is varied and droplet generation is analysed. The change in average pressure at points P_1 , P_2 , and P_c (Fig. 1d) are plotted for changing the width of the side-channel (SC2). Finally, the difference of pressure ($\Delta P = P_1 - P_2$) is analysed with flow time which provides more clarity on the pressure in each side channel during alternate regime in double T-junction device.

Influence of Width of the Main Channel on Droplet Generation

The droplet generation in a single T-junction device was analysed by varying the width of the main channel from 50 μ m to 100 μ m while the width of the side channel is fixed to 50 μ m. The average pressure at points P_c and P_d , the droplet size, droplet generation frequency, and capillary number are noted for varying channel width. The simulation is repeated on a double T-junction device to identify the critical value of “ Λ ” at which droplet generation transits from merging to the alternate regime at the operating flow rates. The pressure difference (ΔP) is analysed with time in a double T-junction device in an alternate regime. The pressure at points P_c , P_1 , and P_2 are plotted for various widths of the main channel.

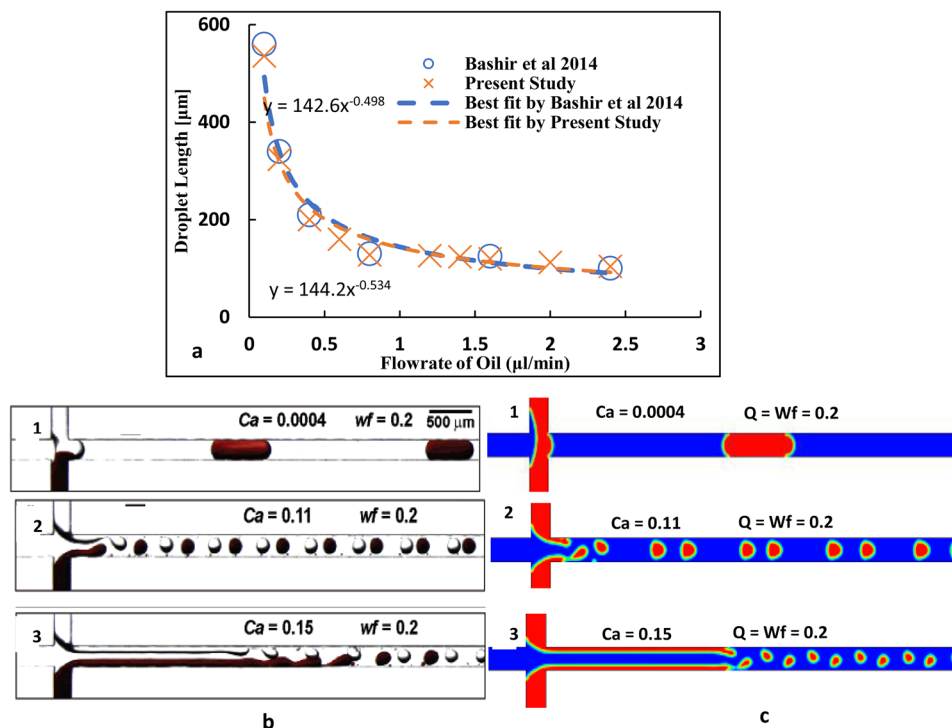
Influence of Surfactant on Alternate Droplet Generation

We study the alternate droplet generation using a double T-junction device whose Λ is set to be at 0.5 (width of both side channels are at 50 μ m and that of the main channel is 100 μ m). The changes due to the addition of surfactant (Span 80) (reducing interfacial tension and increasing contact angle) as mentioned previously are considered on a double T-junction device. The effect of adding surfactant (Span 80) ranging from 0.2% to 4% on droplet generation on a double T-junction device is studied. The simulation study is carried out for both merging and alternate regimes. The pressure difference ΔP ($P_1 - P_2$) is analysed with time and for various surfactant concentrations.

Validation of Simulation Results

The VOF model (single T-junction device) used in the present study is validated with an experimental study (Bashir et al. 2014). The droplet length reduces with an increase in the flowrate of mineral oil. The associated power law to the fitting lines agrees well with each other. Although 3D simulations are important to understand the breakup dynamics of droplets in T-junction devices, the comparative study presented in Fig. 2a with 2D simulation demonstrates a

Fig. 2 Droplet generation in single and double T-junction device. **a** Droplet length versus flowrate of oil at a fixed flowrate of water ($0.2 \mu\text{l}/\text{min}$) in single T-junction device: Comparative study with the experimental results reported by Bashir et al. 2014 at 4% surfactant concentration, **b** Double T-junction device, experimental results from the work of Zheng et al. 2004a, **c** Computational results of the present study. ($Q = W_f =$ water fraction). $\Lambda = 1$ and $\lambda_d = \lambda_c = 16 \text{ mPa}\cdot\text{s}$



qualitative prediction on droplet length at 4% surfactant concentration.

Further, our simulations on alternate droplet generation on a double T-junction device are validated with the experiments done in the past. Figure 2b shows the alternate droplet generation in a double T-junction device by experiment for three different capillary numbers (Zheng et al. 2004a). The simulation results are in close comparison with the experimental data (Fig. 2c). When simulations are validated with experimental data as shown, there can be minor discrepancies associated between the experimental procedures reported and 2D simulations. However, our simulations on alternate droplet generation are reproduced with some consistent geometric scale. This shows that our numerical model is acceptable to study droplet generation in single and double T-junction devices.

Results and Discussion

Effect of Increase in Width of Side-Channel on Droplet Generation

In the case of a single T-junction device, the width of the side channel plays a significant role in droplet generation as it determines the interface area between the two liquid phases (Fig. 1a). The dispersed phase liquid experiences viscous shear force induced by continuous phase liquid at the junction. In our single T-junction device, droplet

generation shifts from dripping to the jetting regime, for the increase in the width of side-channel (W_d) from $50 \mu\text{m}$ to $100 \mu\text{m}$ while the width of the main channel (W_c) is fixed to $100 \mu\text{m}$ (Fig. 3a-f). The length of the droplet produced is proportional to the width of the side channel while the droplet generation frequency does not show any significant change as shown in Fig. 3g. The change in droplet length and frequency, for the increase in width of side-channel, are in good agreement with an earlier study using the Lattice Boltzmann method (Shi et al. 2014). The average pressure at point P_c and P_d increases from 1670 to 1775 Pa and 1750 Pa to 1900 Pa, respectively which is approximately 6% to 8% as the width of the side channel increases from $50 \mu\text{m}$ to $100 \mu\text{m}$ (Fig. 3h). Similarly, the capillary number increases from 0.225 to 0.267 (Fig. 3i) which is approximately 16%.

In the case of a double T-junction device, the width of one of the side channels (SC1) is fixed to $100 \mu\text{m}$ and the width of another side channel (SC2) is increased from $50 \mu\text{m}$ to $100 \mu\text{m}$ (Fig. 1b). In comparison to a single T-junction device, a double T-junction device, contains an additional side-channel. The dispersed phase liquid which flows from this additional side-channel adds to the capillary number and average pressure. The capillary number increases from 0.3 to 0.353 which is approximately 16% and average pressure from 2130 to 2270 Pa which is approximately 7% as the width of the side channel (SC2) increases from $50 \mu\text{m}$ to $100 \mu\text{m}$ (Fig. 3i). When $\Lambda = 1$ ($SC1 = SC2 = 100 \mu\text{m}$), the droplet generation is seen to be in the merging regime (Fig. 3a) until the flow time of

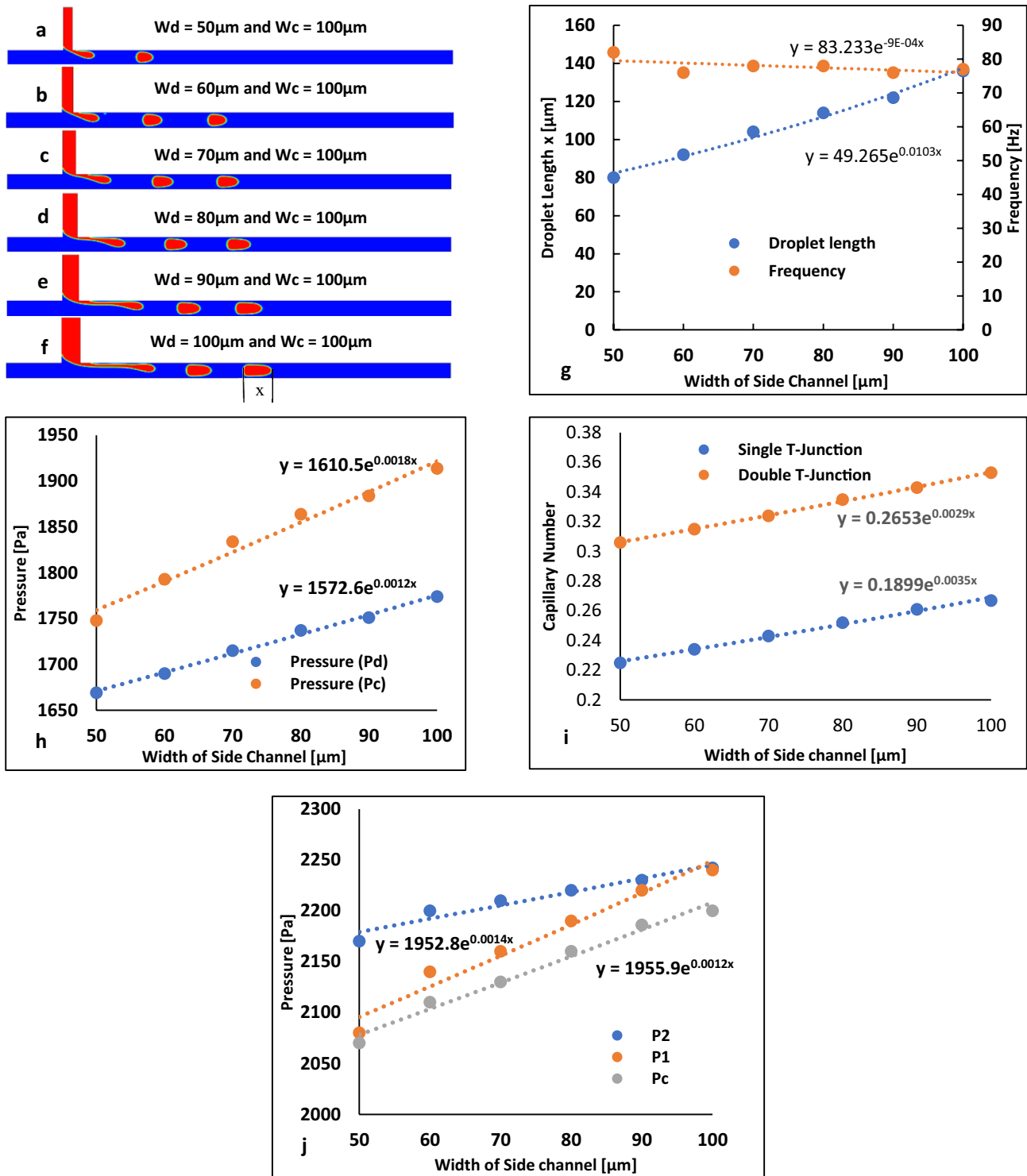


Fig. 3 Effects of increase in the width of side-channel in single T-junction device **a-f** Droplet generation showing the transition from dripping to the jetting regime ("x" represents the droplet length), **g** Droplet length and frequency in single T-junction device, **h**) Pressure at point P_c and P_d in a single T-junction device, **i** Capillary number in

both single and double T-junction devices, **j** Pressure at point P_1 , P_2 and P_c in double T-junction device. [W_d is the width of side-channel in the case of single T-junction and SC1 and SC2 in the case of double T-junction as it contains two side channels: Ref Fig. 1b]

0.05 s, in merging regime, the average pressure in both the side channels are same. With flowtime (> 0.05 s) the pressure starts to vary in both the side channel. This results in the generation of droplets in the alternate regime. In addition, Fig. 3j also shows that during the merging regime, the average pressure in both side channels are the same. Figure 4a shows the droplet generation in the merging regime (flowtime between 0 s to 0.05 s). When the width of $SC2 \leq 90 \mu\text{m}$ droplets are generated in the alternate regime (4b-f). In this case, droplets of different sizes are generated alternatively and the pressure $P_2 > P_1$ (Fig. 1d).

The transition from merging to the alternate regime happens due to the periodic change of pressure between the points P_1 and P_2 . It may be noticed that the average pressure in both the main and side channels in both devices (single and double T-junction) changes and is comparable with the change in the width of the side channel (Fig. 3h and j). Similarly, the increase in capillary number is also comparable in both single and double T-junction devices as shown in Fig. 3i. The distance between the two alternate generating droplets increases with a reduction in the width of one of the side channels (Fig. 4h and i).

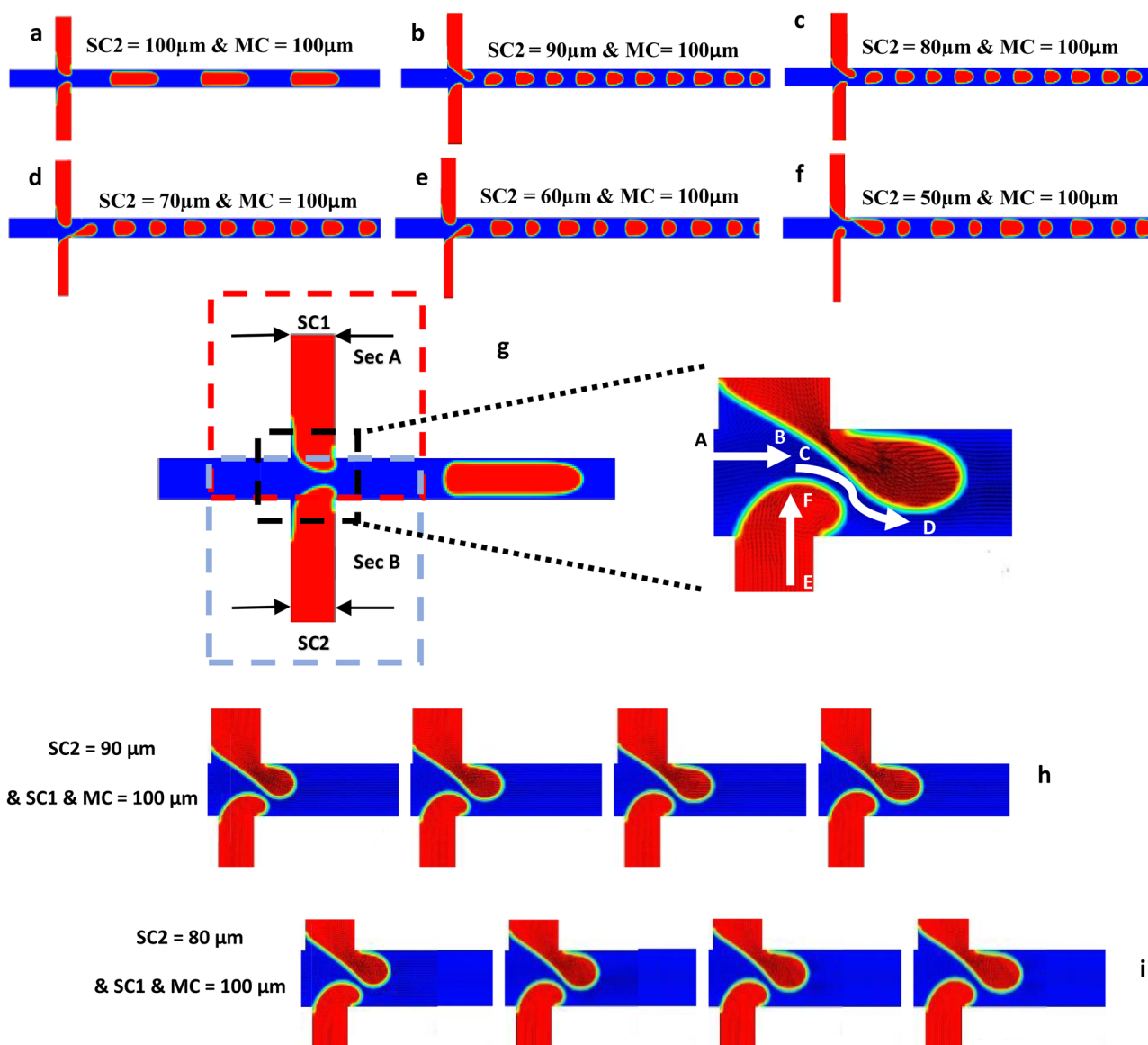


Fig. 4 a-f Droplet generation in double T-junction device for change in the width of SC2 from 100 μm to 50 μm while SC1 is at 100 μm . g Representation of double T-junction device into two sections and deformation of dispersed phase liquid during alternate droplet gen-

eration. h-i The sequence of droplet formation in alternate regime, j-l) The pressure difference (ΔP) Vs time at point P_1 and P_2 for $SC2=90 \mu\text{m}$, $70 \mu\text{m}$, $50 \mu\text{m}$, respectively

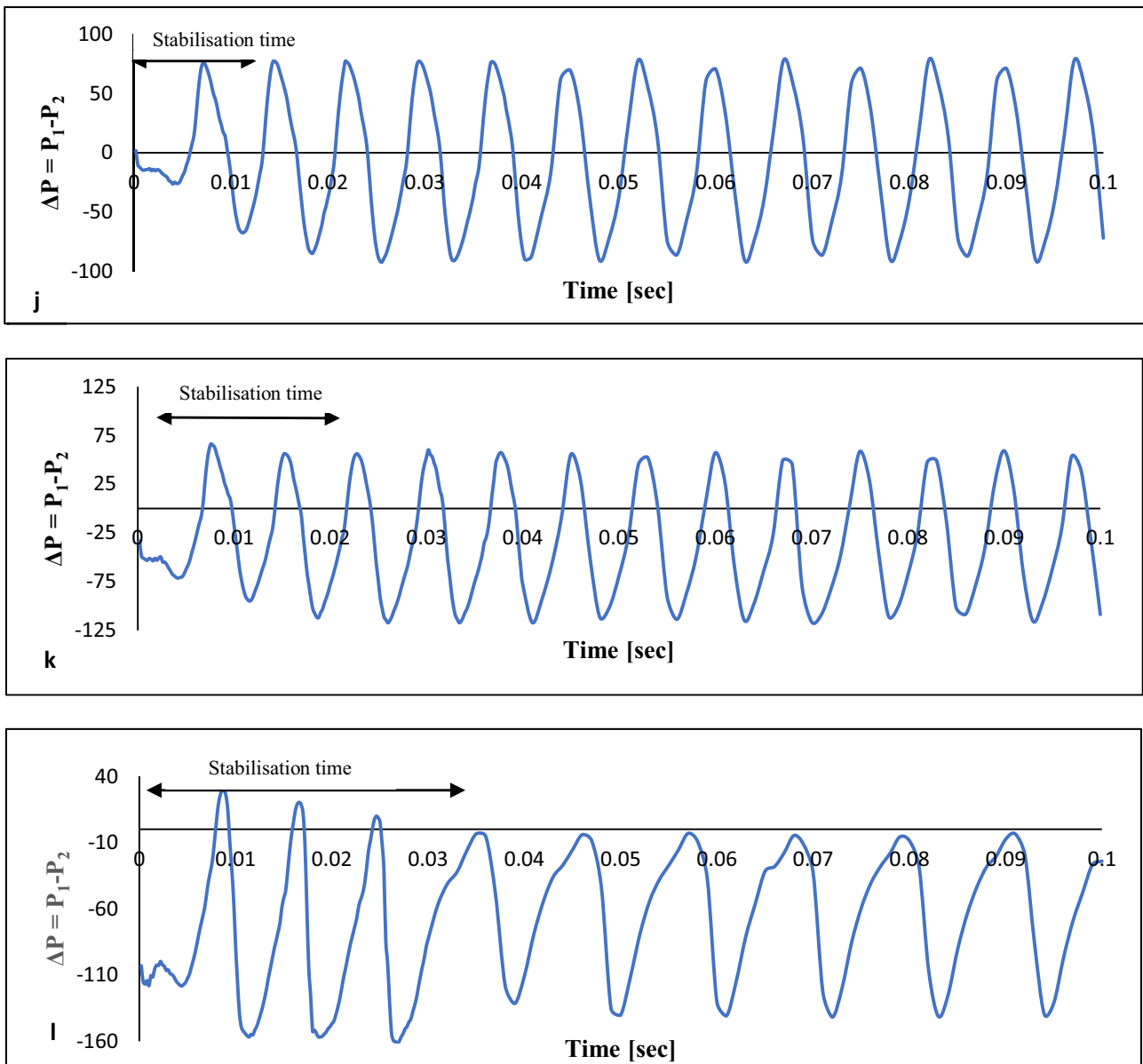


Fig. 4 (continued)

To describe alternate droplet generation, we mark out two regions in the double T-junction device as section A and section B as shown in Fig. 4g. We know that viscous shear force and pressure surrounding the dispersed phase liquid are the two major parameters contributing to droplet generation. When droplets are generated from Section A, the pressure at point P_2 in section B increases, and once the droplet is released in Section A, the dispersed phase liquid in section A pulls back itself into the side channel. This creates a dip in pressure and allows the dispersed phase liquid from Section B to enter the main channel and a droplet is generated. This cycle repeats. But in our case, when the width of side-channel $SC2 < SC1$, the average pressure is always high

in the reducing side channel (SC2) (irrespective of droplet generating side channel), during alternate droplet generation. Thus, it is seen that in the case of asymmetric double T-junction devices, the shear force dominates at the junction with the side-channel having larger width during the droplet generation (Section A in our device) due to the larger fluid interface. This is witnessed by plotting $\Delta P = P_1 - P_2$ with time. When SC2 is 90 μm , 70 μm and 50 μm the peak to peak of ΔP varies between 70 Pa and -90 Pa (Fig. 4j), 60 Pa and -110 Pa (Fig. 4k), and -10 Pa and -140 Pa (Fig. 4l), respectively from its centre reference line with an initial stabilisation time. The time taken by the device to produce sustained droplets in alternate regime is the stabilisation time.

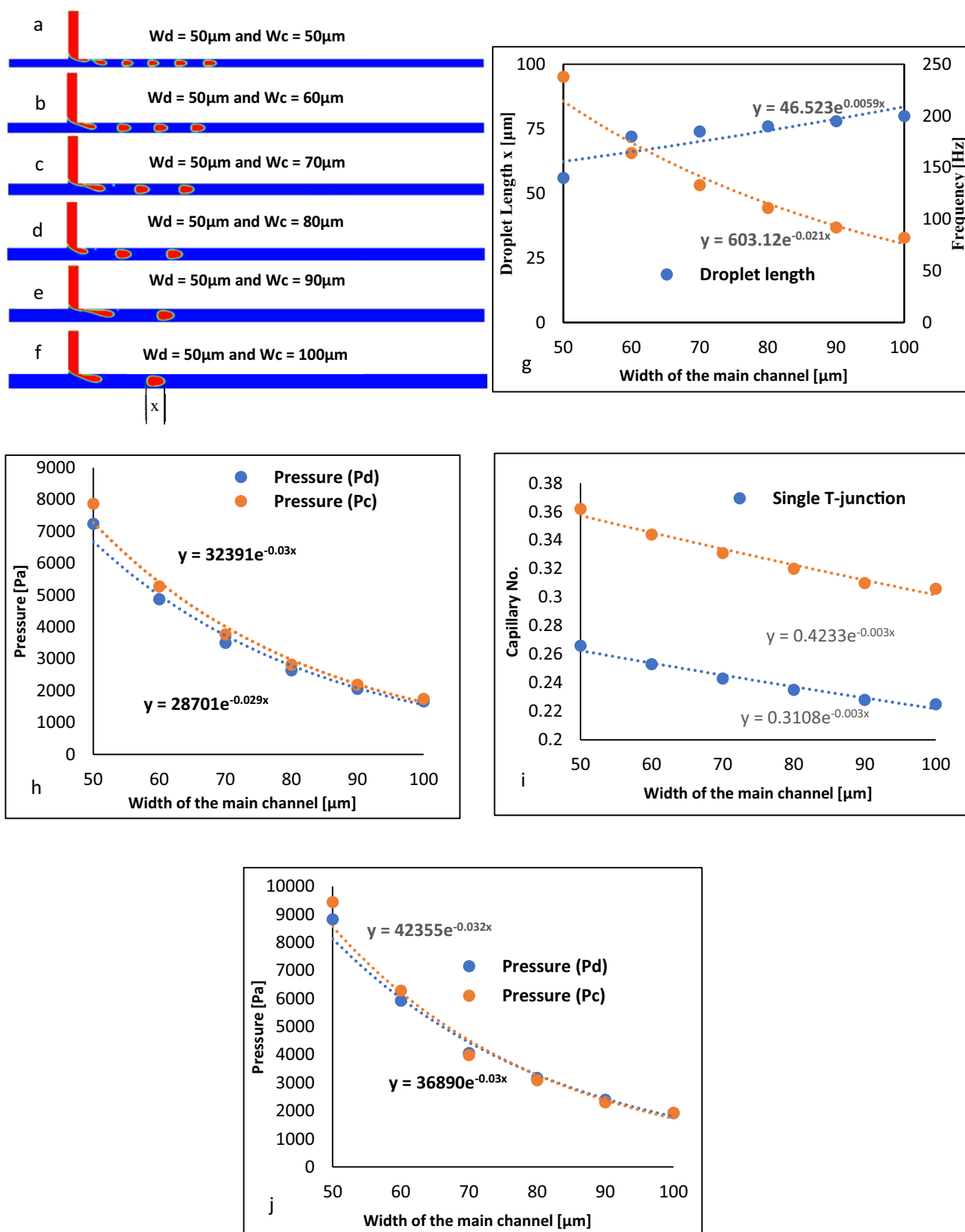


Fig. 5 Effects of increase in the width of the main channel in single T-junction device **a-f** The sequence of droplet generation, (“x” represents the droplet length) **g** Droplet length and frequency, **h** Pressure at

point P_c and P_d , **i** Capillary No. in both single and double T-junction device, **j** Pressure at point P_1 , P_2 and P_c in double T-junction device

This indicates the dominance of pressure of P_2 during the alternate regime when $SC2 < SC1$. In addition, concerning Fig. 4g, the rate of deformation in Section A is higher than in Section B, due to the shearing force in the direction A to B at the larger interface. When dispersed phase liquid deforms in Section A (viscous shear force in C to D), the dispersed phase liquid in section B enters the main channel (E to F) and does not see any deformation until there is a pinch-off in Section A.

Effect of Increase in Width of the Main Channel on Droplet Generation

In contrast to the previous case on a single T-junction device, we study droplet generation by varying the width of the main channel from 50 μm to 100 μm while the width of the side-channel is held constant at 50 μm . The droplet generation remains in the dripping regime as shown in Fig. 5a-f. With the gradual increase in W_c , the droplet length increases and frequency decreases and scales as $l = be^{0.006Wd}$ and $f = ae^{-0.02Wd}$, respectively as shown in Fig. 5g, where “a” and “b” are the parameter specific to device geometry. These results are in good agreement with an earlier study using the Lattice Boltzmann method (Gupta and Kumar 2010). The average pressure at point P_c and P_d approximately decreases from 7870 to 1750 Pa and 7250 Pa to 1750 Pa, respectively as the width of the main channel increases from 50 μm to 100 μm (Fig. 5h) which is approximately 75%. Similarly, the capillary number decreases from 0.267 to 0.225 (Fig. 5i) which is approximately 15%.

In the case of a double T-junction device, the width of the main channel (MC) is increased from 50 μm to 100 μm (Fig. 1b) while both the side channels are fixed at 50 μm . In comparison to a single T-junction device, the pressure and the capillary number increase due to the addition of another side-channel like the previous case. In this case, the capillary number decreases from 0.354 to 0.306 which is approximately 16% (Fig. 5i) and average pressure from 8830 to 1930 Pa which is approximately 78% for the increase in width of the main channel from 50 μm to 100 μm (Fig. 5j). The decrease in average pressure and capillary number in a double T-junction device is in line with the single T-junction device as shown in Fig. 5i. With the gradual increase in the width of the main channel, droplet generation shifts from the merging regime to the alternate regime when the width of the main channel is approximately 1.4 times the width of the side channel (Fig. 6g). There will also be an increase in the distance between the generating droplets at the junction with an increase in the width of the main channel.

The dispersed phase liquid entering the main channel in both sections A and B experience equal viscous shear stress as the width of both the side channel are equal.

The physical behaviour of droplet generation in alternate regimes is analysed by studying the pressure at points P_1 and P_2 with time. When $\Delta P (P_1 - P_2)$ is plotted against time, we see the peak-to-peak pressure switches between -150 Pa to 150 Pa indicating equal dominance of pressure alternatively from each side channel at points P_1 and P_2 over each other (Fig. 6h). These periodic pressure variations prevail for $MC \geq 70 \mu\text{m}$. The periodic pressure variations for $MC = 70 \mu\text{m}$ are shown in Fig. 6h.

Effect of Surfactant on Merging and Alternate droplet formation

In practical applications, the addition of surfactant leads to change in both interfacial tension and wetting (contact angle of the droplet with the channel wall) conditions as mentioned earlier. It was shown that the contact angle of water increased with surfactant concentration, in addition to the reduction in interfacial tension. A similar study has also been the case with other surfactants like SDS (Sodium Dodecyl Sulfate)(Xu et al. 2006), Picosurf (Totlani et al. 2020).

The addition of Span 80 in mineral oil increases the contact angle and reduces the interfacial tension with the gradual increase in its concentration. Bashir et al. (2014) showed that the contact angle increases from 152° to 172° and interfacial tension reduces from 7 to 4 mN when the concentration increases from 0.2% to 4% respectively. We study the droplet generation in a double T-junction device by implementing these changes caused due to the addition of surfactant for the device whose $\Lambda = 0.5$ (Fig. 6f). We study the droplet generation in both merging and alternate regimes for the increasing contact angle and reducing interfacial tension due to the addition of surfactant and increase in its concentration.

Merging of Droplets

To study the effect of surfactant on droplet generation in the merging regime, we set the velocity of V_c and V_d to be 0.004 m/s and 0.002 m/s, respectively (Fig. 7a). In the interest of reporting the results in the merging regime, the velocity of the two liquids has been reduced only in this section to maintain $C_a < 0.02$. The dispersed phase liquid from both the side channel enters the main channel and merge at the junction and pinches off due to the viscous shear force of the continuous phase liquid. The sequence of the merging of two droplets and their release is shown in Fig. 7b. In our case, there is no significant change seen in the droplet generation mechanism with the addition of surfactant (interfacial tension reduces from 7 mN/m to 4 mN/m and increases the contact angle from 152° to 172°). This could

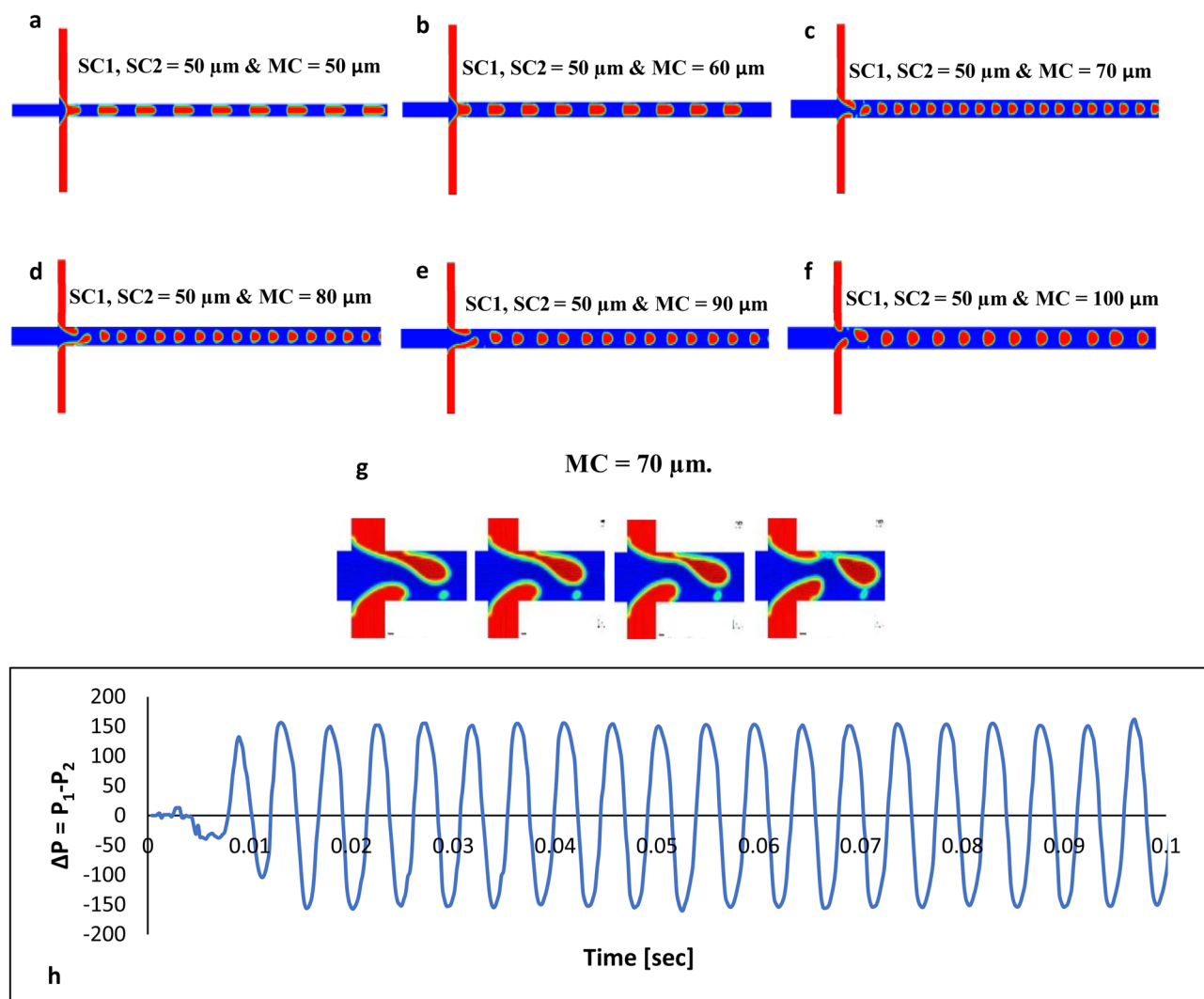


Fig. 6 a-f Droplet generation in double T-junction device for change in the width of the main channel between 50 μm to 100 μm . g The sequence of droplet formation in the alternate regime, for the width of

the main channel at 70 μm , h) ΔP Vs time at point P_1 and P_2 showing the transition from merging regime to the alternate regime (width of MC = 70 μm)

be because the change in the interfacial tension is marginal and though the range of change in contact angle seems fairly good, a numerical study on droplet generation on a single T-junction device shows that the frequency of droplet generation sees a marginal change in generating frequency with increasing contact angle from 100° to 180° for $\lambda < 1$ (Bashir et al. 2011). In our study, we show that it holds even in double T-junction device.

The temporal variation in pressure also provides us more information on droplet generation in the merging regime (Fig. 7c). The number of pressure minima's is equal to the number of droplet releases (in Fig. 7c represents the release of 8 droplets). The pressure at point P_c increases as the dispersed phase liquid enters and blocks the main channel and it drops as the droplet is released. The maximum pressure during the first droplet release was found to be 830 Pa

and it increases to 1000 Pa with time and a stable droplet generation is seen when the surfactant concentration is at 0.2%. The maximum pressure during droplet generation gradually reduces with an increase in surfactant concentration. The maximum pressure during the first droplet release was found to be 780 Pa and it continues to remain the same with time at a surfactant concentration of 4%. The average pressure (plateau region) during the droplet generation decreases with increased surfactant concentration (Fig. 7c). In addition, the average pressure during the droplet generation increases gradually with time as the number of droplet release and stabilizes to a point. When the first droplet exits through the outlet (in our case, in a given length of the main channel, 6 droplets are seen at any given time, so with the generation of 7th droplet, 1st droplet exits through the outlet). This increase in pressure with time is not seen in the

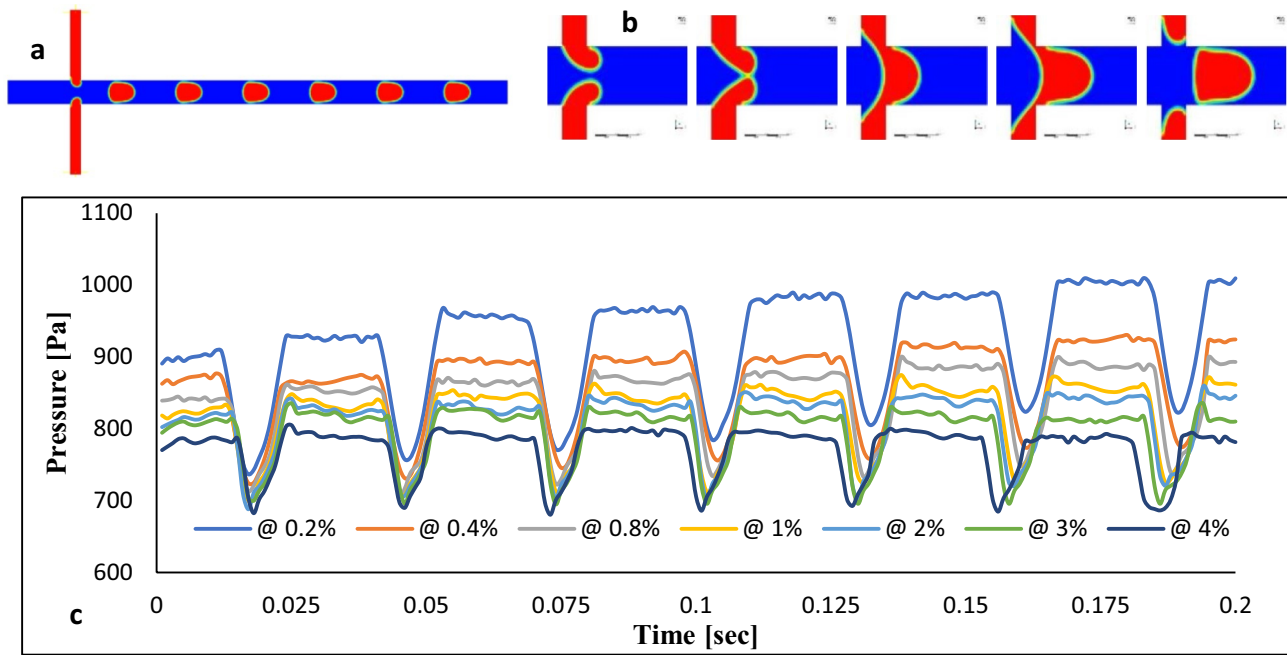


Fig. 7 a Droplet generation in merging regime. b Sequence of Droplet generation in merging regime c Pressure at the dispersed phase liquid inlet Vs Time for various surfactant concentration.

case of increase in surfactant concentration. The frequency of droplet generation can be calculated depending on the droplet release time and it was found to increase marginally from 36 to 42 Hz. The increase in frequency develops with time.

Alternate Droplet Generation

To study droplet generation in an alternate regime, the velocity of the two liquids viz., V_c and V_d are set to 0.02 m/s and 0.01 m/s, respectively. The alternate droplet generation is investigated for an increase in surfactant concentration from 0.2% to 4%. The droplets are generated in the merging regime for surfactant concentration ranging between 0.2% to 0.8%. The pressure at points P_1 and P_2 are the same in the merging regime. Hence the temporal variation of pressure with time overlaps (Fig. 8a). Further increasing the surfactant concentration from 1 to 2%, 3% and 4%, the droplets are generated in alternate regime after 0.04 s, 0.03 s, 0.03 s and 0.0075 s of flow, respectively. This can be seen by plotting ($\Delta P = P_1 - P_2$). During merging regime, ΔP curve ($\Delta P = P_1 - P_2$) is flat. Periodic changes in the pressure between P_1 and P_2 develop with time, and it leads to alternate droplet generation. The flat region in Fig. (8b-d) indicates that the initial droplets are produced in the merging regime.

Conclusion

Numerical investigations were carried out on single and double T-junction microfluidic devices using the Volume of Fluid (VOF) method in 2D. The velocity of continuous phase liquid (mineral oil) and dispersed phase liquid (water) was set to 0.02 m/s and 0.01 m/s, respectively. We initially validate our simulation results with experimental data reported earlier for single T-junction device (Bashir et al. 2014) and double T-junction device (Zheng et al. 2004a). The droplet generation shifts from dripping to a jetting regime with the increase in the width of the side-channel from 50 μm to 100 μm while the width of the main channel was fixed to 100 μm . The frequency of droplet generation reduces marginally from 82 to 77 Hz, and droplet length increases from 80 μm to 135 μm . This change in channel dimensions increases the average pressure in the channel increases from 1670 to 1770 Pa which is approximately 6% to 8% and capillary number from 0.225 to 0.267 which is approximately 16% in the case of a single T-junction device. The addition of a side-channel to the single T-junction device and converting it to double T-junction devices increase overall flow in the device. This is seen when the width of one of the side channels in double T-junction increases from 50 μm to 100 μm , the

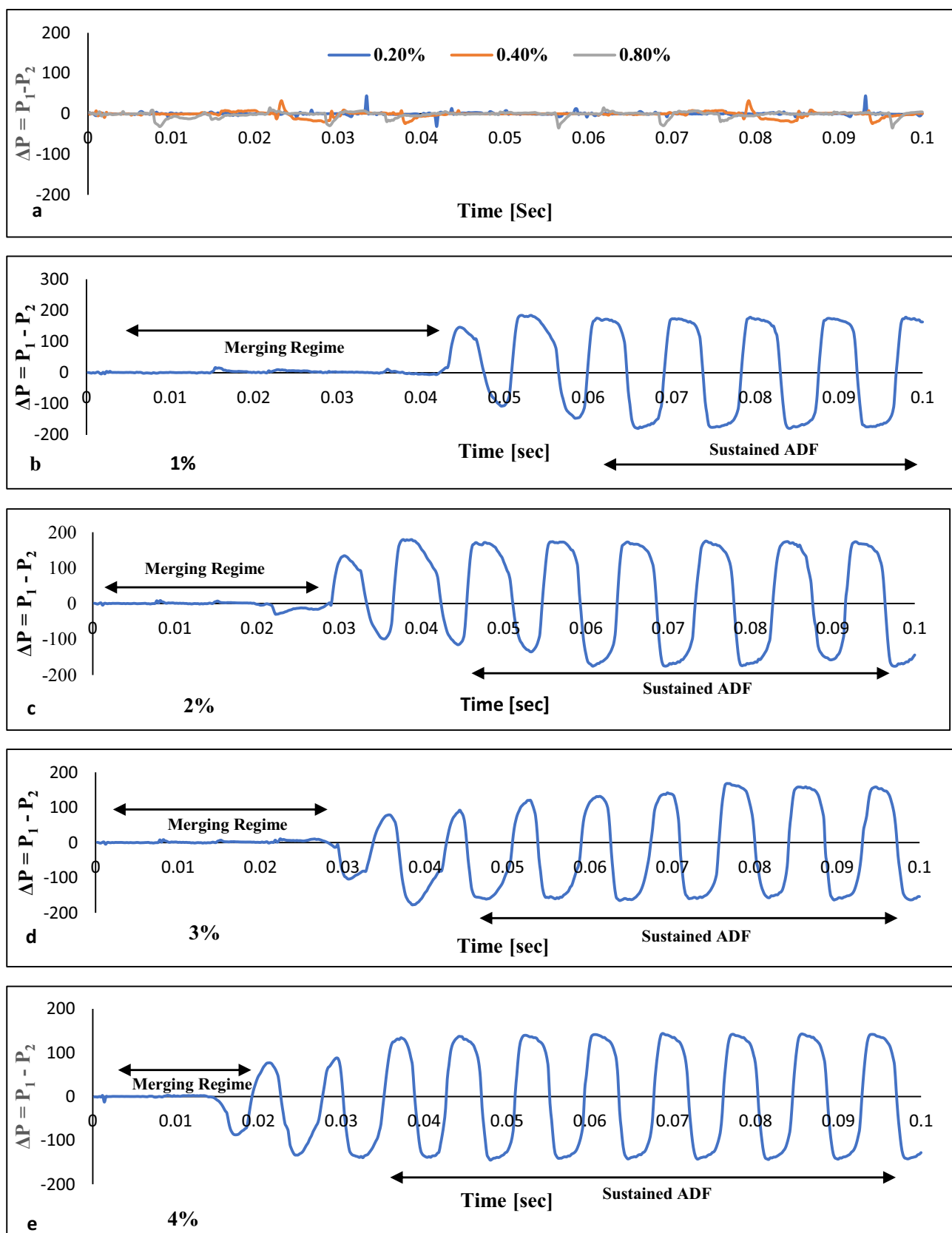


Fig. 8 Pressure Vs time for various surfactant concentration, **a** Difference of pressure ($\Delta P = P_1 - P_2$) Vs time for surfactant concentration of 0.2%, 0.4% and 0.8%, **b-e** for 1%, 2%, 3%, 4% of surfactant concentration, respectively

average pressure increases from 2130 to 2270 Pa, which is approximately 7% and capillary number from 0.306 to 0.353 which is approximately 16%. The pressure variation in both the side channel plotted with time shows that the pressure is higher in the smaller side channel.

The frequency of droplet generation is seen to decrease from 238 to 82 Hz and increase in droplet length from 56 μm to 80 μm for the increase in the width of the main channel from 50 μm to 100 μm while the width of the side-channel is fixed to 50 μm . This increase in the width of the main channel decreases the average pressure from 7870 to 1750 Pa which is approximately 75% and capillary number from 0.267 to 0.225 which is approximately 15%. Similarly, with a change in the width of the main channel in a double T-junction device, the average pressure decreases from 8830 to 1930 Pa which is approximately 78% and the capillary number from 0.354 to 0.306 which is approximately 16%. The gradual increase in width of the main channel also shows that droplet generation shifts from merging regime to alternate droplets regime when the width of the main channel is 1.4 times the width of the side channel. The frequency of droplet generation and droplet length does not significantly change for the increase in the concentration of surfactant (Span 80) from 0.2% to 4% in the merging regime. However, in the case of an alternate regime, it is seen for concentration above 1%.

Declarations

Conflict of Interest The research carried out does not have any financial obligations or attract any conflict of interest.

References

- Amaya-Bower, L., Lee, T.: Lattice Boltzmann simulations of bubble formation in a microfluidic T-junction. *Philosophical Transactions of the Royal Society A: Mathematical, Physical and Engineering Sciences* **369**, 2405–2413 (2011). <https://doi.org/10.1098/rsta.2011.0025>
- Arias, S., Montlaur, A.: Numerical and Experimental Study of the Squeezing-to-Dripping Transition in a T-Junction. *Microgravity Sci Technol* **32**, 687–697 (2020). <https://doi.org/10.1007/s12217-020-09794-z>
- Bashir, S., Rees, J.M., Zimmerman, W.B.: Simulations of microfluidic droplet formation using the two-phase level set method. *Chem Eng Sci* **66**, 4733–4741 (2011). <https://doi.org/10.1016/j.ces.2011.06.034>
- Bashir, S., Solvas, X.C., Bashir, M., et al.: Dynamic wetting in microfluidic droplet formation. *BioChip J* **8**, 122–128 (2014). <https://doi.org/10.1007/s13206-014-8207-y>
- Belousov, K.I., Filatov, N.A., Kukhtevich, I.V., et al.: An asymmetric flow-focusing droplet generator promotes rapid mixing of reagents. *Sci Rep* **11**, 8797 (2021). <https://doi.org/10.1038/s41598-021-88174-y>
- Beneyton, T., Wijaya, I.P.M., Postros, P., et al.: High-throughput screening of filamentous fungi using nanoliter-range droplet-based microfluidics. *Sci Rep* **6**, 1–10 (2016). <https://doi.org/10.1038/srep27223>
- Brackbill, J.U., Kothe, D.B., Zemach, C.: A continuum method for modeling surface tension. *J Comput Phys* **100**, 335–354 (1992). [https://doi.org/10.1016/0021-9991\(92\)90240-Y](https://doi.org/10.1016/0021-9991(92)90240-Y)
- Brouzes, E., Medkova, M., Savenelli, N., et al.: Droplet microfluidic technology for single-cell high-throughput screening. *PNAS* **106**, 14195–14200 (2009). <https://doi.org/10.1073/pnas.0903542106>
- Datta, S.S., Abbaspourrad, A., Amstad, E., et al.: 25th Anniversary Article: Double Emulsion Templated Solid Microcapsules: Mechanics And Controlled Release. *Adv Mater* **26**, 2205–2218 (2014). <https://doi.org/10.1002/adma.201305119>
- Dreyfus, R., Tabeling, P., Willaime, H.: Ordered and Disordered Patterns in Two-Phase Flows in Microchannels. *Phys Rev Lett* **90**, 144505 (2003). <https://doi.org/10.1103/PhysRevLett.90.144505>
- Fidalgo, L.M., Abell, C., Huck, W.T.S.: Surface-induced droplet fusion in microfluidic devices. *Lab Chip* **7**, 984–986 (2007). <https://doi.org/10.1039/B708091C>
- Garstecki, P., Fuerstman, M.J., Stone, H.A., Whitesides, G.M.: Formation of droplets and bubbles in a microfluidic T-junction—scaling and mechanism of break-up. *Lab Chip* **6**, 437–446 (2006). <https://doi.org/10.1039/B510841A>
- Glawdel, T., Ren, C.L.: Droplet formation in microfluidic T-junction generators operating in the transitional regime. III. Dynamic surfactant effects. *Phys Rev E* **86**, 026308 (2012). <https://doi.org/10.1103/PhysRevE.86.026308>
- Gupta, A., Kumar, R.: Flow regime transition at high capillary numbers in a microfluidic T-junction: Viscosity contrast and geometry effect. *Phys Fluids* **22**, 122001 (2010). <https://doi.org/10.1063/1.3523483>
- Gupta, A., Matharoo, H.S., Makkar, D., Kumar, R.: Droplet formation via squeezing mechanism in a microfluidic flow-focusing device. *Comput Fluids* **100**, 218–226 (2014). <https://doi.org/10.1016/j.compfluid.2014.05.023>
- Han, W., Chen, X.: New insights into the pressure during the merged droplet formation in the squeezing time. *Chem Eng Res Des* **145**, 213–225 (2019a). <https://doi.org/10.1016/j.chemd.2019.03.002>
- Han, W., Chen, X.: Effect of Geometry Configuration on the Merged Droplet Formation in a Double T-Junction. *Microgravity Sci Technol* **31**, 855–864 (2019b). <https://doi.org/10.1007/s12217-019-09720-y>
- Hirama, H., Torii, T.: One-to-one encapsulation based on alternating droplet generation. *Sci Rep* **5**, 15196 (2015). <https://doi.org/10.1038/srep15196>
- Hoang, P.H., Dien, L.Q.: Fast synthesis of an inorganic–organic block copolymer in a droplet-based microreactor. *RSC Adv* **4**, 8283–8288 (2014). <https://doi.org/10.1039/C3RA45747H>
- Hong, Y., Wang, F.: Flow rate effect on droplet control in a co-flowing microfluidic device. *Microfluid Nanofluid* **3**, 341–346 (2007). <https://doi.org/10.1007/s10404-006-0134-3>
- Hung, L.-H., Choi, M.K., Tseng, W.-Y., et al.: Alternating droplet generation and controlled dynamic droplet fusion in microfluidic device for CdS nanoparticle synthesis. *Lab Chip* **6**, 174–178 (2006). <https://doi.org/10.1039/B513908B>
- Hung, L.-H., Teh, S.-Y., Jester, J., Lee, A.P.: PLGA micro/nanosphere synthesis by droplet microfluidic solvent evaporation and extraction approaches. *Lab Chip* **10**, 1820–1825 (2010). <https://doi.org/10.1039/C002866E>
- Jin, B.-J., Yoo, J.Y.: Visualization of droplet merging in microchannels using micro-PIV. *Exp Fluids* **52**, 235–245 (2012). <https://doi.org/10.1007/s00348-011-1221-0>
- Kemna, E.W.M., Schoeman, R.M., Wolbers, F., et al.: High-yield cell ordering and deterministic cell-in-droplet encapsulation using

- Dean flow in a curved microchannel. *Lab Chip* **12**, 2881–2887 (2012). <https://doi.org/10.1039/C2LC00013J>
- Kong, T., Wu, J., Yeung, K.W.K., et al.: Microfluidic fabrication of polymeric core-shell microspheres for controlled release applications. *Biomicrofluidics* **7**, 044128 (2013). <https://doi.org/10.1063/1.4819274>
- Lee, T.Y., Choi, T.M., Shim, T.S., et al.: Microfluidic production of multiple emulsions and functional microcapsules. *Lab Chip* **16**, 3415–3440 (2016). <https://doi.org/10.1039/C6LC00809G>
- Leshansky, A.M., Pismen, L.M.: Breakup of drops in a microfluidic T junction. *Phys Fluids* **21**, 023303 (2009). <https://doi.org/10.1063/1.3078515>
- Li, P., Fan, M., Sun, L., et al.: Numerical Simulation of Bubble Formation in a Co-Flowing Liquid in Microfluidic Chip. *Microgravity Sci Technol* **32**, 1–9 (2020). <https://doi.org/10.1007/s12217-019-09729-3>
- Li, X.-B., Li, F.-C., Yang, J.-C., et al.: Study on the mechanism of droplet formation in T-junction microchannel. *Chem Eng Sci* **69**, 340–351 (2012). <https://doi.org/10.1016/j.ces.2011.10.048>
- Liu, H., Zhang, Y.: Droplet formation in a T-shaped microfluidic junction. *J Appl Phys* **106**, 034906 (2009). <https://doi.org/10.1063/1.3187831>
- Liu, K., Qin, J.: Droplet-fused microreactors for room temperature synthesis of nanoscale needle-like hydroxyapatite. *Nanotechnology* **24**, 125602 (2013). <https://doi.org/10.1088/0957-4484/24/12/125602>
- Nasser, G.A., Fath El-Bab, A.M.R., Abdel-Mawgood, A.L., et al.: CO2 Laser Fabrication of PMMA Microfluidic Double T-Junction Device with Modified Inlet-Angle for Cost-Effective PCR Application. *Micromachines* **10**, 678 (2019). <https://doi.org/10.3390/mi10100678>
- Nekouei, M., Vanapalli, S.A.: Volume-of-fluid simulations in microfluidic T-junction devices: Influence of viscosity ratio on droplet size. *Phys. Fluids* **29**, 032007 (2017). <https://doi.org/10.1063/1.4978801>
- Ngo, I.-L., Dang, T.-D., Byon, C., Joo, S.W.: A numerical study on the dynamics of droplet formation in a microfluidic double T-junction. *Biomicrofluidics* **9**, 024107 (2015). <https://doi.org/10.1063/1.4916228>
- Nunes, J.K., Tsai, S.S.H., Wan, J., Stone, H.A.: Dripping and jetting in microfluidic multiphase flows applied to particle and fiber synthesis. *J Phys D Appl Phys* **46** (2013). <https://doi.org/10.1088/0022-3727/46/11/114002>
- O'Brien, C.M., Rood, K.D., Bhattacharyya, K., et al.: Capture of circulating tumor cells using photoacoustic flowmetry and two phase flow. *JBO* **17**, 061221 (2012). <https://doi.org/10.1117/1.JBO.17.6.061221>
- Peng, L., Yang, M., Guo, S., et al.: The effect of interfacial tension on droplet formation in flow-focusing microfluidic device. *Biomed Microdevices* **13**, 559–564 (2011). <https://doi.org/10.1007/s10544-011-9526-6>
- Saqib, M., Şahinoğlu, O.B., Erdem, E.Y.: Alternating Droplet Formation by using Tapered Channel Geometry. *Sci Rep* **8**, 1–9 (2018). <https://doi.org/10.1038/s41598-018-19966-y>
- Seo, M., Paquet, C., Nie, Z., et al.: Microfluidic consecutive flow-focusing droplet generators. *Soft Matter* **3**, 986–992 (2007). <https://doi.org/10.1039/B700687J>
- Shi, Y., Tang, G.H., Xia, H.H.: Lattice Boltzmann simulation of droplet formation in T-junction and flow focusing devices. *Comput Fluids* **90**, 155–163 (2014). <https://doi.org/10.1016/j.compfluid.2013.11.025>
- Song, H., Li, H.-W., Munson, M.S., et al.: On-Chip Titration of an Anticoagulant Argatroban and Determination of the Clotting Time within Whole Blood or Plasma Using a Plug-Based Microfluidic System. *Anal Chem* **78**, 4839–4849 (2006). <https://doi.org/10.1021/ac0601718>
- Soroor, M., Zabetian Targhi, M., Tabatabaei, S.A.: Numerical and experimental investigation of a flow focusing droplet-based microfluidic device. *Eur J Mech B Fluids* **89**, 289–300 (2021). <https://doi.org/10.1016/j.euromechflu.2021.06.013>
- Surya, H.P.N., Parayil, S., Banerjee, U., et al.: Alternating and merged droplets in a double T-junction microchannel. *BioChip J* **9**, 16–26 (2015). <https://doi.org/10.1007/s13206-014-9103-1>
- Tadros, T.F.: Emulsion Formation, Stability, and Rheology. In: Emulsion Formation and Stability. John Wiley & Sons, Ltd, 1–75 (2013)
- Totlani, K., Hurkmans, J.-W., van Gulik, W.M., et al.: Scalable microfluidic droplet on-demand generator for non-steady operation of droplet-based assays. *Lab Chip* **20**, 1398–1409 (2020). <https://doi.org/10.1039/C9LC01103J>
- Um, E., Lee, D.-S., Pyo, H.-B., Park, J.-K.: Continuous generation of hydrogel beads and encapsulation of biological materials using a microfluidic droplet-merging channel. *Microfluid Nanofluid* **5**, 541–549 (2008). <https://doi.org/10.1007/s10404-008-0268-6>
- Vivek, R.: Computational Flow Modeling for Chemical Reactor Engineering, Volume 5 - 1st Edition (2019). <https://www.elsevier.com/books/computational-flow-modeling-for-chemical-reactor-engineering/ranade/978-0-12-576960-0>. Accessed 24 Nov 2019
- Wojnicki, M., Luty-Błocho, M., Hessel, V., et al.: Micro Droplet Formation towards Continuous Nanoparticles Synthesis. *Micromachines* **9**, 248 (2018). <https://doi.org/10.3390/mi9050248>
- Xu, J.H., Li, S.W., Tan, J., et al.: Preparation of highly monodisperse droplet in a T-junction microfluidic device. *AIChE J* **52**, 3005–3010 (2006). <https://doi.org/10.1002/aic.10924>
- Yan, Y., Guo, D., Wen, S.Z.: Numerical simulation of junction point pressure during droplet formation in a microfluidic T-junction. *Chem Eng Sci* **84**, 591–601 (2012). <https://doi.org/10.1016/j.ces.2012.08.055>
- Yesiloz, G., Boybay, M.S., Ren, C.L.: Label-free high-throughput detection and content sensing of individual droplets in microfluidic systems. *Lab Chip* **15**, 4008–4019 (2015). <https://doi.org/10.1039/C5LC00314H>
- Zhang, Y., Jiang, H.-R.: A review on continuous-flow microfluidic PCR in droplets: Advances, challenges and future. *Anal Chim Acta* **914**, 7–16 (2016). <https://doi.org/10.1016/j.aca.2016.02.006>
- Zheng, B., Tice, J.D., Ismagilov, R.F.: Formation of Droplets of Alternating Composition in Microfluidic Channels and Applications to Indexing of Concentrations in Droplet-Based Assays. *Anal Chem* **76**, 4977–4982 (2004a). <https://doi.org/10.1021/ac0495743>
- Zheng, B., Tice, J.D., Roach, L.S., Ismagilov, R.F.: A Droplet-Based, Composite PDMS/Glass Capillary Microfluidic System for Evaluating Protein Crystallization Conditions by Microbatch and Vapor-Diffusion Methods with On-Chip X-Ray Diffraction. *Angew Chem Int Ed* **43**, 2508–2511 (2004b). <https://doi.org/10.1002/anie.200453974>

Publisher's Note Springer Nature remains neutral with regard to jurisdictional claims in published maps and institutional affiliations.